Silver Nanoparticle Loaded TiO2 Nanotubes with High Photocatalytic and Antibacterial Activity Synthesized by Photoreduction Method

Article *in* Journal of Photochemistry and Photobiology A Chemistry · October 2017

DOI: 10.1016/j.jphotochem.2017.10.051

CITATIONS
5

READS
103

7 authors, including:

Viet Van Pham
Ho Chi Minh City University of Science
24 PUBLICATIONS **52** CITATIONS
SEE PROFILE

Thang Phan
Sungkyunkwan University
41 PUBLICATIONS **174** CITATIONS
SEE PROFILE

Shinya Maenosono
Japan Advanced Institute of Science and Technology
145 PUBLICATIONS **2,533** CITATIONS
SEE PROFILE

Cao Minh Thi
Ho Chi Minh City University of Technology (HUTECH)
68 PUBLICATIONS **295** CITATIONS
SEE PROFILE

Journal of Photochemistry and Photobiology A: Chemistry 352 (2018) 106–112

Contents lists available at ScienceDirect

Journal of Photochemistry and Photobiology A: Chemistry

journal homepage: www.elsevier.com/locate/jphotochem

Silver nanoparticle loaded TiO_2 nanotubes with high photocatalytic and antibacterial activity synthesized by photoreduction method

Pham Van Viet[a,*], Bach Thang Phan[a], Derrick Mott[b], Shinya Maenosono[b], Truong Tan Sang[c], Cao Minh Thi[c], Le Van Hieu[a,*]

[a] Nanomaterials for Environmental Applications Laboratory, Faculty of Materials Science and Technology, University of Science, VNU–HCMC, 227 Nguyen Van Cu Street, District 5, Ho Chi Minh City, 700000, Vietnam
[b] School of Materials Science, Japan Advanced Institute of Science and Technology, 1–1 Asahidai, Nomi, Ishikawa 923–1292, Japan
[c] CM Thi Laboratory, Ho Chi Minh City University of Technology (HUTECH), 475A Dien Bien Phu Street, Binh Thanh District, Ho Chi Minh City, 700000, Vietnam

ARTICLE INFO

Article history:
Received 26 July 2017
Received in revised form 25 October 2017
Accepted 26 October 2017
Available online 2 November 2017

Keywords:
Silver nanoparticles
TiO_2 nanotubes
Photoreduction
Photocatalyst
Sunlight

ABSTRACT

Silver nanoparticles (Ag NPs) were loaded on TiO_2 nanotubes (TNTs) *via* photoreduction method at room temperature without any additional reducing agent. The morphology and crystal structure were examined by transmission electron microscopy, X–ray diffraction pattern, and Raman spectroscopy. Chemical states of silver, titanium, and oxygen were analyzed by X–ray photoelectron spectroscopy. The results showed that Ag NPs with an average diameter of 5 nm were uniformly distributed on TNTs surface. Ag NPs improved both photocatalytic and the antibacterial activity of TNTs under sunlight irradiation. Ag/TNTs decomposed 81.2% of methylene blue and 75.8% of methylene orange after 150 min under sunlight irradiation. In addition, Ag/TNTs at 20 ppm concentration eliminated 99.99% of *Staphylococcus aureus* after 60 min under sunlight irradiation. This research demonstrated that Ag/TNTs can be synthesized at industrial scale by the photoreduction method and are effective antibacterial materials.

1. Introduction

Recently, the use of semiconductors with solar irradiation to deal with environmental problems is drawing a lot of attention. Reducing the size of the semiconductors will modify their physical, chemical, or biological properties, especially under irradiation [1]. Among these various semiconductors at the nanoscale, TiO_2 nanotubes (TNTs) have been used widely to remove polluted organic chemicals and bacteria in the water because this material has high specific surface area and chemical stability. Moreover, TNTs are low cost and non-toxic [2,3]. However, the photocatalytic applications of TNTs under sunlight have been limited because of their relatively wide band gap (about ~3.78 eV at room temperature) and high electron–hole recombination rate [4–6].

To overcome these obstacles, many researchers have focused on loading a noble metal (i.e. Au, Pt, Pd, Ag) onto TNTs because *(i)* these nanoparticles expand the absorption range to the visible region by the surface plasmon resonance effect [7,8] and *(ii)* act as electron trappers to reduce the rate of electron–hole recombination [9,10]. Among noble metals at the nanoscale, Ag is an attractive candidate to enhance the activity of TNTs because in comparison to other noble metals, Ag has the strongest conductivity and electron trapping ability [2], is not very expensive, can be used on the industrial scale, and is non-toxic for humans at low concentration. Therefore, to improve the photocatalytic activity of TNTs, this project will focus on loading Ag NPs on TNTs.

Many methods were investigated to synthesize Ag/TNTs, such as chemical reduction, sputtering deposition, microwave-assisted method, photoreduction, etc. Most of these techniques require many kinds of chemicals and must be conducted at high temperature. However, the photoreduction method uses water as a solvent, does not need any reducing agent or stabilizer, and can be carried out at room temperature.

Over the past a few years, loading of Ag NPs onto hydrothermally synthesized TNTs is usually accomplished by photoreduction from a UV source, showing good results. However, the previous studies indicated that the synthesis processes must use a UV lamp with high power (from 400 to 500 W) [11,12] or make use of many assistant chemicals, such as HNO_3, NaOH, N_2 or Ar gas, ect [13,12,11], or the product must be treated at a temperature of at least 400 °C [14].

* Corresponding authors.
E-mail addresses: pvviet@hcmus.edu.vn (P.V. Viet), lvhieu@hcmus.edu.vn (L.V. Hieu).

https://doi.org/10.1016/j.jphotochem.2017.10.051
1010-6030/

These disadvantages in synthesis process prevent the application of Ag/TNTs in industrial scale. To overcome these obstacles, we tried to fabricate Ag/TNTs by a simple photoreduction procedure, in which does not use any additional chemicals and can be carried out at room temperature.

2. Materials and methods

2.1. Chemicals

TNTs were synthesized by the hydrothermal method [15]. Silver nitrate (99.9%) was purchased from Alpha Chemika, India. Methylene blue (MB, 99%) was purchased from JHD Fine Chemicals, China. Methylene Orange (MO, 99%) was purchased from Xilong Scientific, China. Deionized (DI) water was supplied by a Puris–Evo water system.

2.2. Preparation of Ag/TNTs

Various publications about Ag/TiO_2 indicated that 2.0 wt.% of Ag exhibited the highest photocatalytic activity [16–18]. Therefore, we decided to fabricate Ag/TNTs with 2.0 wt.% Ag. First, 0.0425 g $AgNO_3$ was added into a 100 mL DI. Then, the solution was magnetically stirred with 1.0 g TNT powder. Then, the mixture was constantly stirred and irradiated under a UVC lamp (OSRAM, Germany, 18 W, 254 nm) for 24 h. Finally, the product was filtered, washed with DI water, and dried at 100 °C for 2 h.

2.3. Material characterization

The crystal structure of the materials was determined by X–ray diffraction (XRD) pattern (Bruker D8 Advance 5005, Cu Kα with λ = 0.154064 nm). Vibration modes of bonds in the materials were

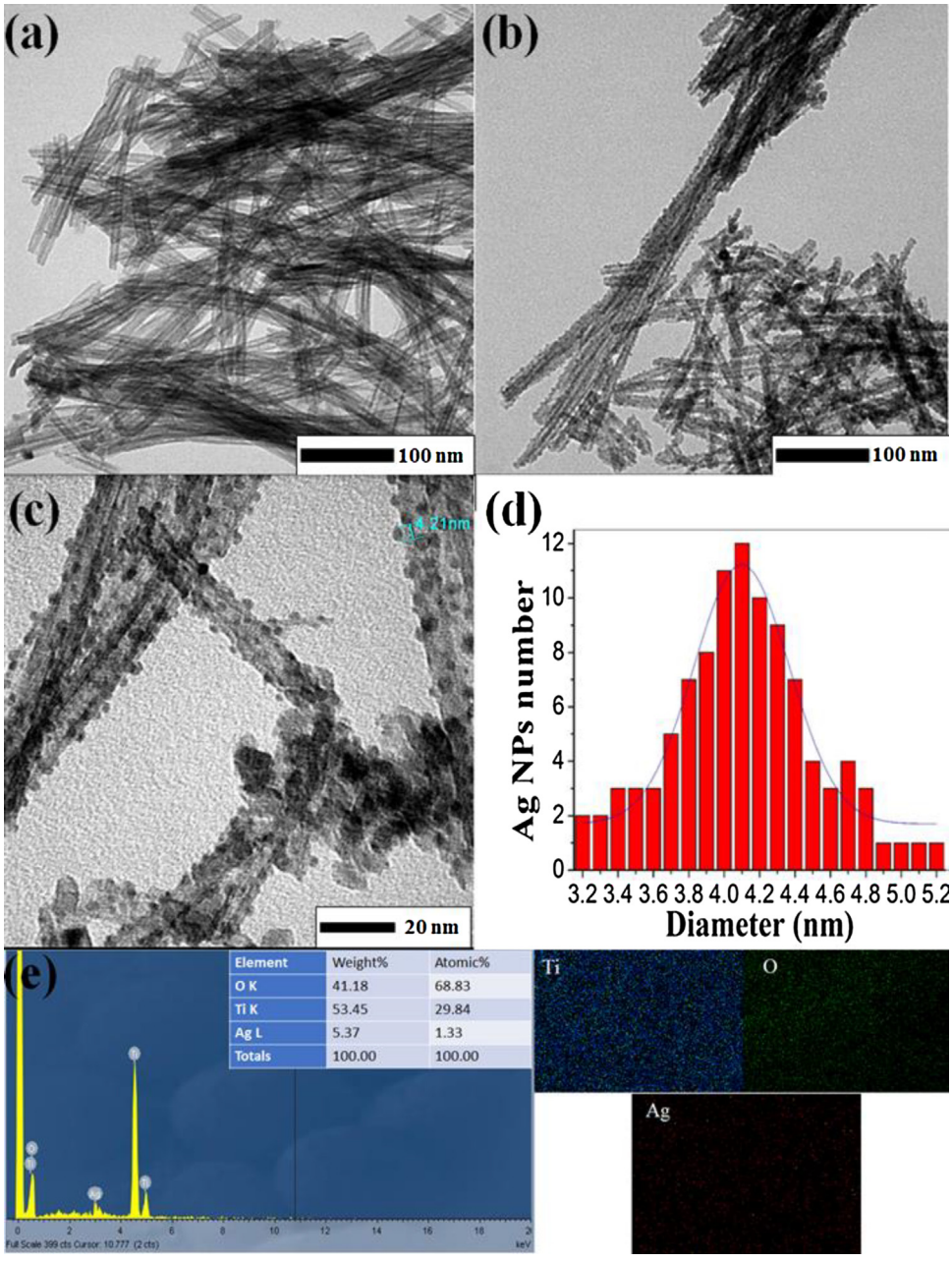

Fig. 1. TEM images of TNTs (a), Ag/TNTs with 100 nm of scale bar (b), 50 nm of scale bar (c), size distribution of Ag NPs (d), and EDS of Ag/TNTs (e).

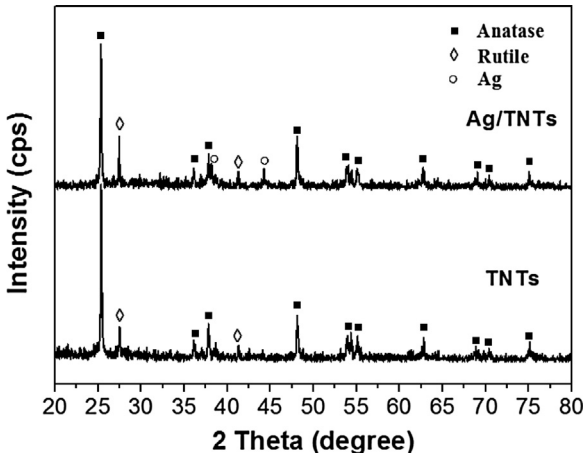

Fig. 2. XRD patterns of materials.

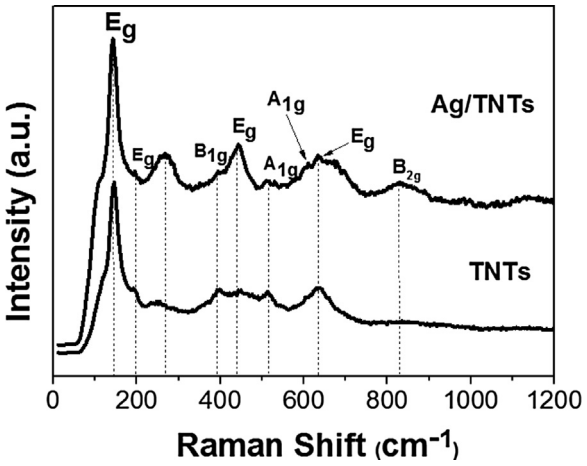

Fig. 3. Raman spectra of materials.

detected by Raman spectroscopy (Jobin Yvon–Labram 300 spectrometer, excitation source: He–Ar laser with λ = 514.5 nm). The morphology of the materials was recorded by transmission electron microscopy (TEM) image (JEM 1400 instrument). Energy dispersive X-ray spectroscopy (EDS) mapping technique was used to determine the weight and the atomic percentage of elements in the material using a JEOL S4800. The chemical states of silver, titanium, and oxygen in the materials were analyzed by X–ray photoelectron spectroscopy (XPS) pattern (Perkin–Elmer RBD upgraded PHI–5000C ESCA system with monochromatic Mg–Kα excitation, and the charge neutralizer was used to investigate the surface electronic states of the materials).

2.4. Photocatalytic activity of materials

The photocatalytic activity of the materials was evaluated by the degradation efficiency of MB and MO (organic polluted indicators) solutions under sunlight. 60 mL of MB/MO at 20 mg/L and 0.02 g of catalyst were magnetically stirred for 60 min in the dark for equilibrium of the adsorption/desorption process of MB on the materials to be achieved. Then the mixture was subjected to sunlight irradiation. The absorption spectrum of the MB/MO solution was regularly recorded every 30 min of irradiation. The experiments were carried out from 10:00 to 13:00 o'clock on a sunny day (35–40 °C) at Ho Chi Minh city, Vietnam. All the

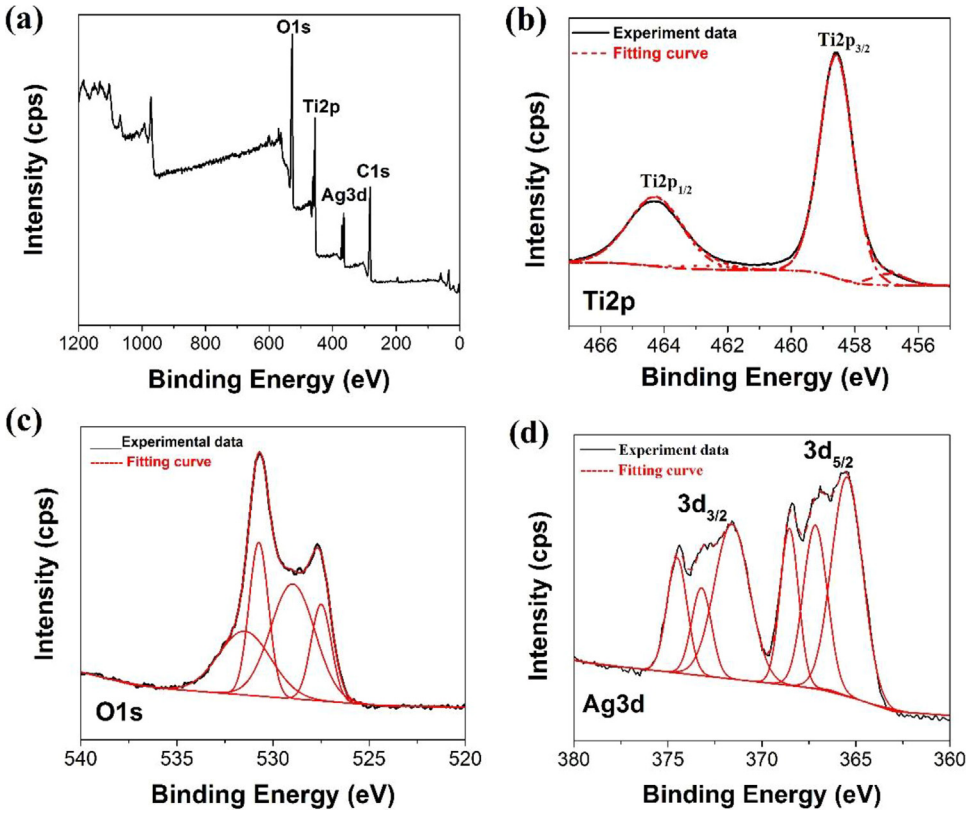

Fig. 4. XPS of Ag/TNTs (a) and HRXPS of Ti_{2p} (b), O_{1s} (c), and Ag_{3d} (d).

Table 1
XPS data for the oxidation state and content of Ag in Ag 3d.

Oxidation statements	Peak position and content	
	BE (eV)	%
Ag^0 $3d_{3/2}$	374.5	11.6
Ag^0 $3d_{5/2}$	368.5	13.5
Ag^+ $3d_{3/2}$	371.6	25.2
Ag^+ $3d_{5/2}$	365.5	30.5
Ag^{2+} $3d_{3/2}$	373.1	4.8
Ag^{2+} $3d_{5/2}$	367.2	14.3

experiments were repeated 3 times. The photocatalytic degradation efficiency, η, was calculated as $\eta\,(\%) = 100 \times (C_0 - C_t)/C_0$, where C_0 and C_t were the concentrations of MB/MO before and t min after sunlight exposure, respectively. MB and MO in the supernatants were measured with a UV–vis absorption spectra (U2910, HITACHI, Japan) at wavelengths of 664 nm and 464 nm, respectively.

2.5. The antibacterial activity of materials

Staphylococcus aureus (*S. aureus*) was incubated at 37 °C for 24 h (2.4×10^8 CFU/mL) and was used to study the antibacterial activity of the materials. The antibacterial activity of materials was tested in the dark and under sunlight from 11:00 AM to 12:00 PM in Ho Chi Minh city, Vietnam.

In the dark, TNTs and Ag/TNTs at a concentration of 20 ppm, 50 ppm, and 100 ppm were added separately into 6 Petri dishes. A Petri dish was left blank as the control sample. The bacteria concentrations were recorded after 30 min of incubation. As the same with the investigation of the antibacterial activity under sunlight irradiation, TNTs at 20 ppm and Ag/TNTs at 20 ppm were added separately into 2 Petri dishes, and a dish was left blank in the same condition as the control sample. These Petri dishes were exposed under sunlight irradiation for 60 min. After the illuminated period, the bacteria were incubated for 24 h in the dark. The bacteria concentrations were recorded after the incubation.

3. Results and discussion

3.1. Morphology and structure of materials

3.1.1. TEM observation

The TEM images were used to characterize the surface morphology of Ag NPs, TNTs and Ag/TNTs. Fig. 1 shows that the average size of Ag NPs is about 3–5 nm and Ag NPs are uniformly deposited on the TNT surface. After the photoreduction process, TNTs maintained their original morphology with an outer diameter of 8 ± 2 nm, an inner diameter of 6 ± 2 nm, and length ranging from 200 to 400 nm. Fig. 1(e) shows that the material is high purify and is mainly composed of Ti, O and Ag. Because the O: Ti atom ratio (~2.3) is bigger than 2. Therefore, the product can exist a silver oxide.

3.1.2. XRD characterization

As reported by Fig. 2, all samples exhibited diffraction characteristics at 25.0°, 36.95°, 38.5°, 48.2°, 55.3°, and 75.0°, corresponding to (101), (004), (200), (105), and (204). planes of the anatase phase, respectively (JCPDS No.65-5714). The diffraction peaks at 38.2° and 44.4° corresponds to (111) and (200) plane of Ag NPs' face centered cubic crystal (JCPDS No.65-2871) [8,19]. Diffraction characteristic at 27.45° corresponds to (110) plane of the rutile phase (JCPDS No.21-1276). The significant increase in this

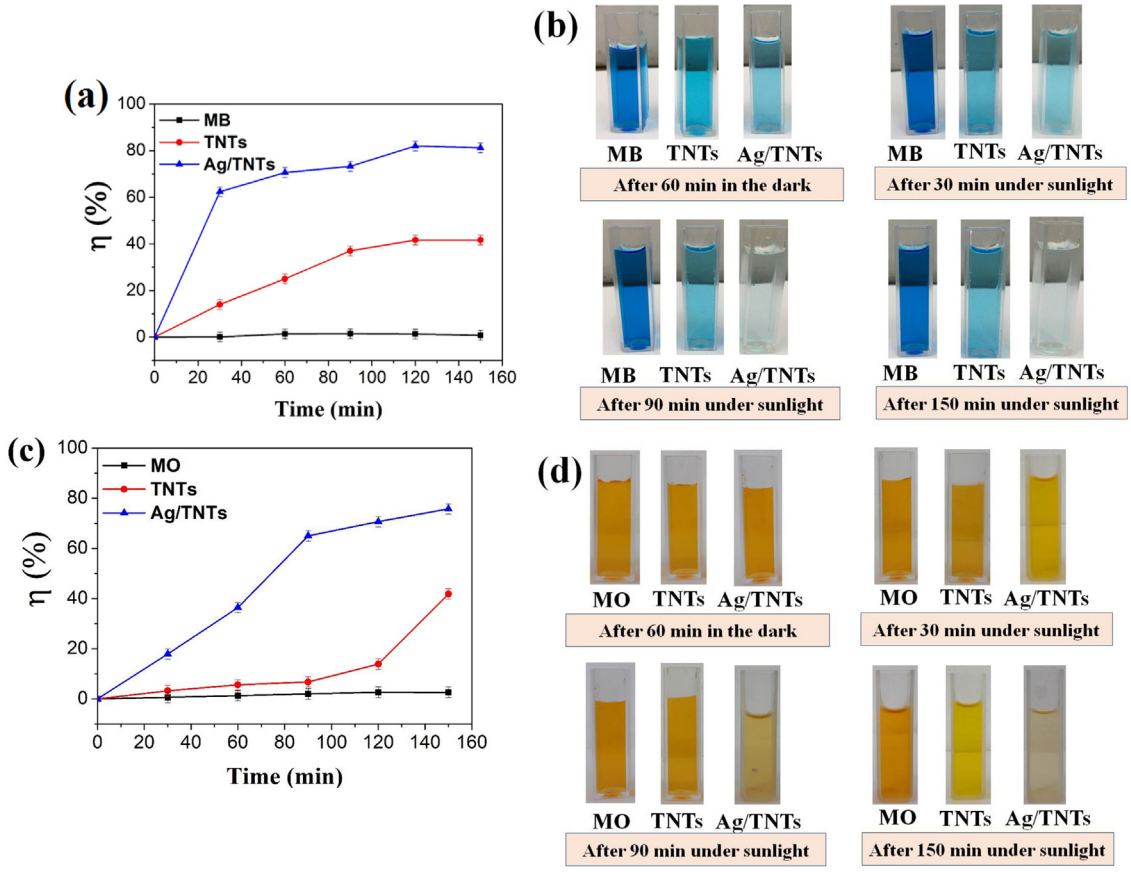

Fig. 5. MB and MO photodegradation efficiency (a-c) of materials under sunlight irradiation and the change of color along dye degrade process (b-d).

peak's intensity in Ag/TNTs could be explained by the fact that Ag NPs absorbed additional heat to improve the formation of rutile phase [20].

3.1.3. Raman analysis

Raman spectra of TNTs show six active modes of the anatase phase, representing three E_g modes with centered–peak around 142 ($E_{g(1)}$), 196 ($E_{g(2)}$), and 641 ($E_{g(3)}$) cm^{-1}; two B_{1g} modes at 395 ($B_{1g(1)}$) and 513 ($B_{1g(2)}$) cm^{-1}; and one A_{1g} mode at 513 cm^{-1} [21,22] (Fig. 3). Besides these modes, three modes at 440 (E_g), 613.8 (A_{1g}), and 828.7 (B_{2g}) cm^{-1} of rutile phase [23,22] are also observed. The E_g, B_{1g}, and A_{1g} were contributed by the symmetric stretching vibration, the symmetric bending vibration, and the anti-symmetric bending vibration of O-Ti-O in TiO_2, respectively. However, the increase in the intensity of the peak at 271 cm^{-1}, corresponding to Ti—O—H group [24,25] in Ag/TNTs can be explained by the fact that the O-Ti-O group reacts with water on TNTs to form a Ti—O—H group in the photoreduction process.

3.1.4. XPS characterization

Fig. 4a shows XPS of Ag/TNTs, including binding energy peaks for Ti, O, and Ag. The carbon is attributed to adventitiously adsorbed hydrocarbons. The high–resolution Ti 2p XPS spectrum (Fig. 4(b)) shows two binding energy (BE) peaks at 459.4 and 465 eV, corresponding to Ti^{4+} in TiO_2 [26]. The BE peak at 456.4 eV corresponds to Ti^{3+} [27]. The O 1 s XPS spectrum (Fig. 4(c)) shows a major BE peak at 531 eV, characterizing to O^{2-} in TiO_2, and a smaller peak at 528 eV, characterizing to O— [11,28]. Fig. 4(d) shows that the Ag/TNT sample contains three states of Ag, namely, Ag^0, Ag^+, and Ag^{2+}, including two BE peaks at 374.5 and 368.5 eV, corresponding to Ag $3d_{3/2}$ and Ag $3d_{5/2}$ of Ag^0, respectively [29,30]. The BE peaks at 373.1 and 367.2 eV correspond to Ag $3d_{3/2}$ and Ag $3d_{5/2}$ of Ag^{2+}, respectively [30]. Furthermore, there were two BE peaks at 371.6 and 365.5 eV, corresponding to Ag $3d_{3/2}$ and Ag $3d_{5/2}$ of Ag^+, respectively. The Ag^0 state exists about 25.1%, Ag^{2+} is 19.1%, and Ag^+ state dominates with more than 50% (Table 1). These results are explained by the fact that the photoreduction process usually contains oxygen and ozone gases, so they oxidized from Ag^0 to form Ag^+ and Ag^{2+} states [31,32].

3.2. The photocatalytic activity of materials

Ag/TNTs have the superior photocatalytic potential of TNTs in the photodegradation of both dyes (MB and MO). The MB and MO photodegradation efficiency of Ag/TNTs is approximately double that of TNTs after 150 min under sunlight irradiation. Detailly, the MB (MO) photodegradation efficiencies of TNTs and Ag/TNTs are 41.7% (41.8%) and 81.2% (75.8%), respectively (Fig. 5(a)–(c)).

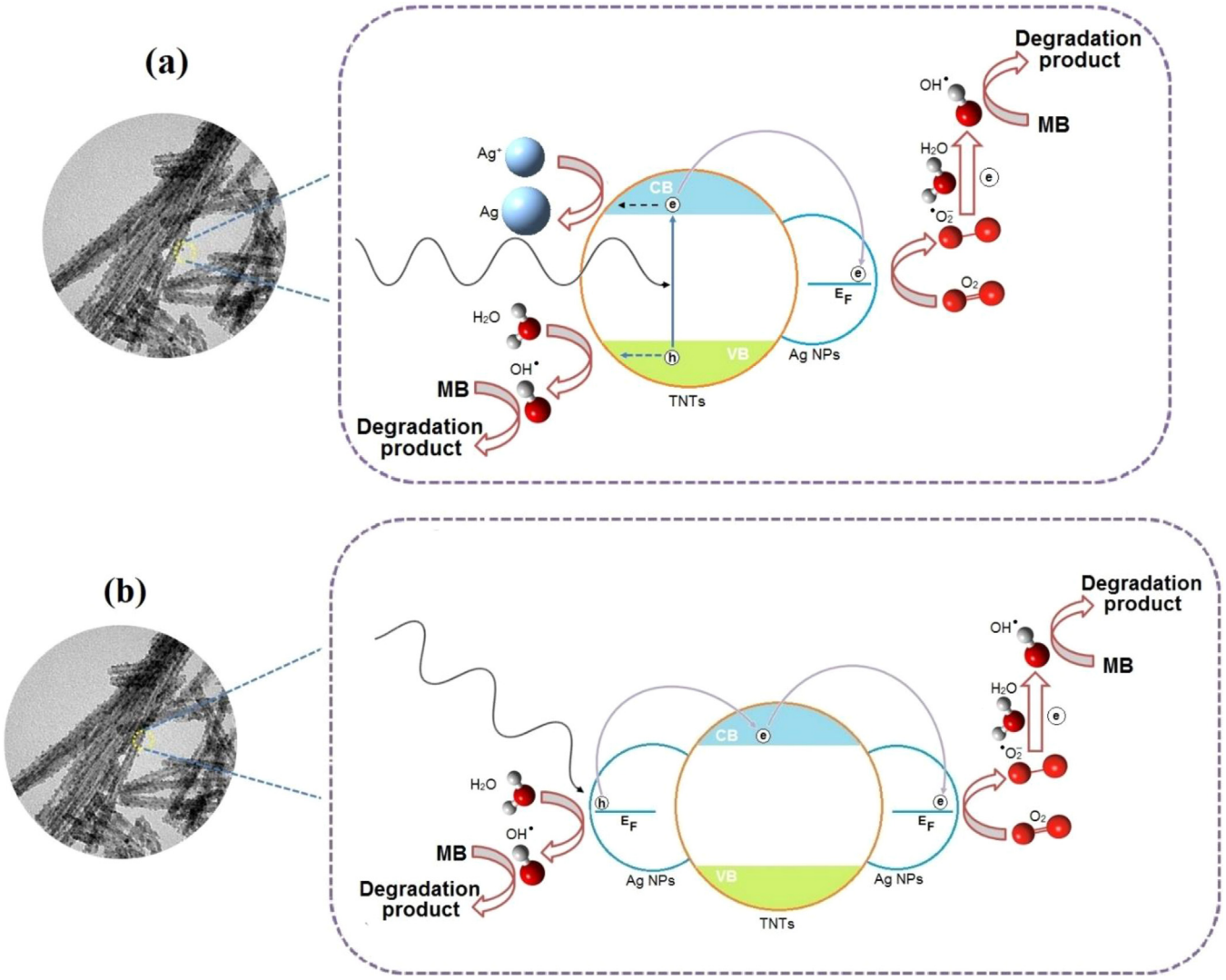

Fig. 6. Photocatalytic mechanism of Ag/TNTs under UV light (a) and visible light (b).

Table 2
Antibacterial efficiency of TNTs and Ag/TNTs with various concentration under the dark and sunlight irradiation.

Concentration (ppm)	Antibacterial efficiency (%)			
	Dark		Light	
	TNTs	Ag/TNTs	TNTs	Ag/TNTs
100	86.55	99.37	N/A	N/A
50	75.33	97.37	N/A	N/A
20	55.68	92.67	95.9	99.99

In addition, dyes degradation also expresses through change of dyes color (Fig. 5(b) and (d)). The color of MB and MO almost do not change during the irradiation process while the color of solution with the presence of TNTs catalyst has faded but they are not much compared to the original dyes color. Clearly, the change a lot of color of solution with the presence of Ag/TNTs catalyst from blue and orange to transparent can be observed after 150 min under sunlight irradiation.

3.3. Photocatalytic mechanism of Ag/TNTs

The photocatalytic reaction of Ag/TNTs could be activated by UV light or visible light (Fig. 6), which both exist in sunlight.

Under UV light (Fig. 6(a)), the electrons in the valence band (VB) of TNTs moved to the conduction band (CB) and were isolated with the holes by the heterojunction structure between Ag NPs and TNTs [33–35]. Then, these electrons reduced O_2 on Ag NPs to $^{\bullet}O_2^-$ [36]. These radicals could receive more electrons to become *OH*. Meanwhile, the holes in the VB oxidized water on TNTs to the $OH^{\bullet}$ free radical. Next, $^{\bullet}O_2^-$ and $OH^{\bullet}$ will oxidize MB/MO to the degradation products.

It is also worth to note that the electron and hole recombination can be suppressed by Ag^+ ion. Ag^+ can inhibits this process because of its high reduction potential. Under sunlight condition, the transformation of Ag^+ is shown in equations below [37]:

$$Ag^+ + e_{CB}^- \rightarrow Ag^0$$

Photo-generated electrons are captured by Ag^+ species, which are then reduced into Ag^0 (Fig. 6(a)). The contribution of silver does not stop here, it also can suppress the electron-hole recombination by Schottky barrier [38]. Consequently, the synergic effect of the oxidation states of silver (including two BE peaks at 371.6 and 365.5 eV as Fig. 4 (c)) significantly enhance the photocatalytic performance of Ag/TNTs material [39].

Under visible light (Fig. 6(b)), electrons on the surface of Ag NPs resonated (by surface plasmon resonance effect) and became plasmonically excited. Next, they moved to the CB of TNTs, and were further trapped by neighboring Ag NPs. As under UV light irradiation, these electrons then reduced O_2 on TNTs to $^{\bullet}O_2^-$ anion radical, and the holes in Ag NPs oxidized water on Ag NPs to $OH^{\bullet}$. After that, $^{\bullet}O_2^-$ and $OH^{\bullet}$ radicals will oxidize MB/MO to the degradation products.

3.4. The antibacterial activity of the materials

Table 2 shows that in the dark conditions, the antibacterial activity of TNTs is very strong with 86.55% of antibacterial efficiency at 100 ppm concentration after 60 min of incubation. Alternately, the antibacterial activity decreases when the concentration of TNTs is decreased. On the other hand, Ag/TNTs exhibited stable antibacterial activity under dark conditions. The antibacterial efficiency of Ag/TNTs in the dark reached 92.67 to 99.27% for Ag/TNTs concentration from 20 to 100 ppm. The antibacterial mechanism of TNTs in the dark is mainly based on the generation of reactive oxygen species (ROS) (hydroxyl radicals ($OH^{\bullet}$), superoxide anion ($^{\bullet}O_2^-$), and hydrogen peroxide (H_2O_2), which were the product of the reaction between Ti^{3+} and O^- vacancies with water and oxygen on the TNT surface [40–43]. The presence of Ti^{3+} and O^- in the materials was confirmed by XPS spectrum (Fig. 4b, c). Furthermore, the presence of the Ag^+ state (about 50% in Ag/TNTs sample) can eliminate the bacteria by destructing bacteria' membrane, interaction with protein thiol groups, and/or damage to their DNA [31,43–46].

Fig. 7 shows the antibacterial activities against *S. aureus* of TNTs and Ag/TNTs under sunlight irradiation. After 24 h of sunlight irradiation the *S. aureus* bacteria in the control sample grew fully on a petri dish (Fig. 7a). Compared to the antibacterial activity of Ag/TNTs, the antibacterial activity of TNTs is lower because the number of bacteria in this dish only decreased partly (Fig. 7b). When Ag NPs are incorporated with TNTs, their antibacterial activity is improved. This showed that Ag/TNTs with 20 ppm concentration showed inhibitory zones (Fig. 7c). The antibacterial efficiency of TNTs, and Ag/TNTs under sunlight irradiation are 95.90 and 99.99%, respectively. Compared to the dark condition, both the antibacterial activity of TNTs and Ag/TNTs were both improved under sunlight irradiation, and the antibacterial activity of Ag/TNTs was better than that of TNTs. This enhancing of the antibacterial activity of the materials was also explained by the generation of the ROS when the materials were excited by sunlight irradiation. This result is consistent with the photocatalytic mechanism of Ag/TNTs which was mentioned the above.

4. Conclusions

Ag NPs were loaded on a TNT surface by the photoreduction method at room temperature without any additional reducing agent. Ag NPs have the average particle size from about 3 to 5 nm

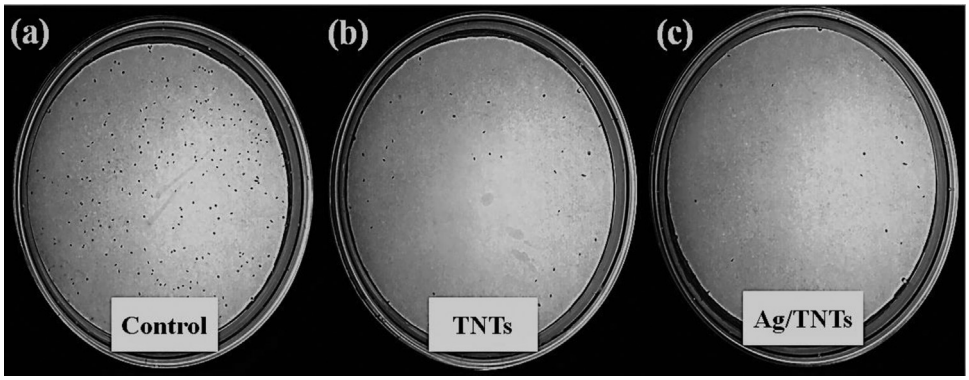

Fig. 7. Antibacterial activities against *S. aureus*: (a) control sample, b) TNTs, and (c) Ag/TNTs under sunlight irradiation.

and are uniformly deposited on the TNT surface. Ag NPs significantly improved the photocatalytic activity and the antibacterial activity of TNTs. Moreover, the photocatalytic efficiency of Ag/TNTs was twice that of TNTs after 150 min under sunlight irradiation. Ag/TNTs at 20 ppm concentration eliminated 99.99% of *S. aureus* after 60 min under sunlight irradiation. The photocatalytic and antibacterial activity of Ag/TNTs was attributed to $OH^{\bullet}$, $^{\bullet}O_2^-$, and H_2O_2, which generated under sunlight, degrade MB/MO and eliminate bacteria. Ag/TNTs synthesized by simple photoreduction method might be a promise material for treating polluted water in the future.

Conflict of interest

The authors have declared no conflict of interest.

Acknowledgments

The authors would especially like to record their gratitude to the Administrator Board of University of Science, Vietnam National University Ho Chi Minh City for supporting facilities. We thank Dr. Pham Minh Nhut (HUTECH, Vietnam) and Ms. Nguyen Ho Ngoc Bich (HUTECH, Vietnam) for the support to measure the antibacterial characteristics of materials.

References

[1] P. Roy, S. Berger, P. Schmuki, TiO_2 nanotubes: synthesis and applications, Angewandte Chemie 50 (2011) 2904–2939.
[2] C. Xu, P. Chen, J. Liu, H. Yin, X. Gao, X. Mei, Fabrication of visible-light-driven Ag/TiO_2 heterojunction composites induced by shock wave, J. Alloys Compd. 679 (2016) 463–469.
[3] H. Chaker, L. Chérif-Aouali, S. Khaoulani, A. Bengueddach, S. Fourmentin, Photocatalytic degradation of methyl orange and real wastewater by silver doped mesoporous TiO_2 catalysts, J. Photochem. Photobiol. A: Chem. 318 (2016) 142–149.
[4] D.V. Bavykin, S.N. Gordeev, A.V. Moskalenko, A.A. Lapkin, F.C. Walsh, Apparent two-dimensional behavior of TiO_2 nanotubes revealed by light absorption and luminescence, J. Phys. Chem. B 109 (2005) 8565–8569.
[5] J. Tao, T. Luttrell, M. Batzill, A two-dimensional phase of TiO(2) with a reduced bandgap, Nat. Chem. 3 (2011) 296–300.
[6] A. Ayati, A. Ahmadpour, F.F. Bamoharram, B. Tanhaei, M. Manttari, M. Sillanpaa, A review on catalytic applications of Au/TiO_2 nanoparticles in the removal of water pollutant, Chemosphere 107 (2014) 163–174.
[7] L. Jiang, G. Zhou, J. Mi, Z. Wu, Fabrication of visible-light-driven one-dimensional anatase TiO_2/Ag heterojunction plasmonic photocatalyst, Catal. Commun. 24 (2012) 48–51.
[8] Z. Lian, W. Wang, S. Xiao, X. Li, Y. Cui, D. Zhang, G. Li, H. Li, Plasmonic silver quantum dots coupled with hierarchical TiO_2 nanotube arrays photoelectrodes for efficient visible-light photoelectrocatalytic hydrogen evolution, Sci. Rep. 5 (2015) 10461.
[9] J. Ma, M. Yang, Y. Sun, C. Li, Q. Li, F. Gao, F. Yu, J. Chen, Fabrication of Ag/TiO_2 nanotube array with enhanced photo-catalytic degradation of aqueous organic pollutant, Physica. E 58 (2014) 24–29.
[10] M.Z. Ge, C.Y. Cao, S.H. Li, Y.X. Tang, L.N. Wang, N. Qi, J.Y. Huang, K.Q. Zhang, S.S. Al-Deyab, Y.K. Lai, In situ plasmonic Ag nanoparticle anchored TiO_2 nanotube arrays as visible-light-driven photocatalysts for enhanced water splitting, Nanoscale 8 (2016) 5226–5234.
[11] L. Yu, X. Yang, Y. Ye, X. Peng, D. Wang, Silver nanoparticles decorated anatase TiO_2(2) nanotubes for removal of pentachlorophenol from water, J. Colloid Interface Sci. 453 (2015) 100–106.
[12] Q. Zhao, M. Li, J. Chu, T. Jiang, H. Yin, Preparation, characterization of Au (or Pt)-loaded titania nanotubes and their photocatalytic activities for degradation of methyl orange, Appl. Surf. Sci. 255 (2009) 3773–3778.
[13] H. Li, X. Duan, G. Liu, X. Liu, Photochemical synthesis and characterization of Ag/TiO_2 nanotube composites, J. Mater. Sci. 43 (2008) 1669–1676.
[14] L. Zong, Q. Li, J. Zhang, X. Wang, J. Yang, Preparation of Pd-loaded La-doped TiO_2 nanotubes and investigation of their photocatalytic activity under visible light, J. Nanopart. Res. 15 (2013) 2042.
[15] P.V. Viet, B.T. Phan, L.V. Hieu, C.M. Thi, The effect of acid treatment and reactive temperature on the formation of TiO_2 nanotubes, J. Nanosci. Nanotechnol. 15 (2015) 5202–5206.
[16] J. Ma, Z. Xiong, T. David Waite, W.J. Ng, X.S. Zhao, Enhanced inactivation of bacteria with silver-modified mesoporous TiO_2 under weak ultraviolet irradiation, Microporous Mesoporous Mater. 144 (2011) 97–104.
[17] V. Jovic, P.H. Hsieh, W.T. Chen, D.S. Waterhouse, T. Söhnel, G.I.N. Waterhouse, Photocatalytic H_2 production from ethanol over Au/TiO_2 and Ag/TiO_2, Int. J. Nanotechnol. 11 (2014) 686.
[18] X. You, F. Chen, J. Zhang, M. Anpo, A novel deposition precipitation method for preparation of Ag-loaded titanium dioxide, Catal. Lett. 102 (2005) 247–250.
[19] Y.Q. Liang, Z.D. Cui, S.L. Zhu, Y. Liu, X.J. Yang, Silver nanoparticles supported on TiO_2 nanotubes as active catalysts for ethanol oxidation, J. Catal. 278 (2011) 276–287.
[20] D.A.H. Hanaor, C.C. Sorrell, Review of the anatase to rutile phase transformation, J. Mater. Sci. 46 (2010) 855–874.
[21] O.A.D. Gallardo, R. Moiraghi, M.A. Macchione, J.A. Godoy, M.A. Pérez, E.A. Coronado, V.A. Macagno, Silver oxide particles/silver nanoparticles interconversion: susceptibility of forward/backward reactions to the chemical environment at room temperature, RSC Adv. 2 (2012) 2923.
[22] Y. Ji, Growth mechanism and photocatalytic performance of double-walled and bamboo-type TiO_2 nanotube arrays, RSC Adv. 4 (2014) 40474–40481.
[23] J.S. Kim, S.S. Shin, H.S. Han, S. Shin, J.H. Suk, K. Kang, K.S. Hong, I.S. Cho, Facile preparation of TiO_2Nanobranch/Nanoparticle hybrid architecture with enhanced light harvesting properties for dye-Sensitized solar cells, J. Nanomater. 2015 (2015) 1–9.
[24] P. Ramasamy, D.-H. Lim, J. Kim, J. Kim, A general approach for synthesis of functional metal oxide nanotubes and their application in dye-sensitized solar cells, RSC Adv. 4 (2014) 2858–2864.
[25] B.C. Viana, O.P. Ferreira, A.G. Souza Filho, C.M. Rodrigues, S.G. Moraes, J. Mendes Filho, O.L. Alves, Decorating titanate nanotubes with CeO2Nanoparticles, J. Phys. Chem. C 113 (2009) 20234–20239.
[26] D. Sethi, N. Jada, R. Kumar, S. Ramasamy, S. Pandey, T. Das, J. Kalidoss, P.S. Mukherjee, A. Tiwari, Synthesis and characterization of titania nanorods from ilmenite for photocatalytic annihilation of E coli, J. Photochem. Photobiol. B Biol. 140 (2014) 69–78.
[27] D. Gonbeau, C. Guimon, G. Pfister-Guillouzo, A. Levasseur, G. Meunier, R. Dormoy, XPS study of thin films of titanium oxysulfides, Surf. Sci. 254 (1991) 81–89.
[28] J. Zhu, F. Chen, J. Zhang, H. Chen, M. Anpo, Fe3+-TiO_2 photocatalysts prepared by combining sol–gel method with hydrothermal treatment and their characterization, J. Photochem. Photobiol. A: Chem. 180 (2006) 196–204.
[29] M. Romand, M. Roubin, J.-P. Deloume, X-ray photoelectron emission studies of mixed selenides $AgGaSe_2$ and Ag_9GaSe_6, J. Solid State Chem. 25 (1978) 59–64.
[30] V.K. Kaushik, XPS core level spectra and Auger parameters for some silver compounds, J. Electron Spectrosc. Relat. Phenom. 56 (1991) 273–277.
[31] X. Zhang, M. Li, X. He, X. Huang, R. Hang, B. Tang, Effects of silver concentrations on microstructure and properties of nanostructured titania films, Mater. Des. 65 (2015) 600–605 (1980-2015).
[32] M.L. Zheludkevich, A.G. Gusakov, A.G. Voropaev, A.A. Vecher, E.N. Kozyrski, S.A. Raspopov, Oxidation of silver by atomic oxygen, Oxid. Met. 61 (2004) 39–48.
[33] D. Yang, Y. Sun, Z. Tong, Y. Tian, Y. Li, Z. Jiang, Synthesis of Ag/TiO_2Nanotube heterojunction with improved visible-Light photocatalytic performance inspired by bioadhesion, J. Phys. Chem. C 119 (2015) 5827–5835.
[34] C. He, D. Shu, M. Su, D. Xia, A. Mudar Abou, L. Lin, Y. Xiong, Photocatalytic activity of metal (Pt, Ag, and Cu)-deposited TiO_2 photoelectrodes for degradation of organic pollutants in aqueous solution, Desalination 253 (2010) 88–93.
[35] D. Kong, J.Z.Y. Tan, F. Yang, J. Zeng, X. Zhang, Electrodeposited Ag nanoparticles on TiO_2 nanorods for enhanced UV visible light photoreduction CO2 to CH4, Appl. Surf. Sci. 277 (2013) 105–110.
[36] E. Kowalska, O.O. Mahaney, R. Abe, B. Ohtani, Visible-light-induced photocatalysis through surface plasmon excitation of gold on titania surfaces, Phys. Chem. Chem. Phys.: PCCP 12 (2010) 2344–2355.
[37] L. Xu, D. Zhang, L. Ming, Y. Jiao, F. Chen, Synergistic effect of interfacial lattice Ag(+) and Ag(0) clusters in enhancing the photocatalytic performance of TiO_2, Phys. Chem. Chem. Phys.: PCCP 16 (2014) 19358–19364.
[38] Y. Wang, L. Liu, L. Xu, C. Meng, W. Zhu, Ag/TiO_2 nanofiber heterostructures: highly enhanced photocatalysts under visible light, J. Appl. Phys. 113 (2013) 174311.
[39] Y. Chen, Y. Xie, J. Yang, H. Cao, Y. Zhang, Reaction mechanism and metal ion transformation in photocatalytic ozonation of phenol and oxalic acid with Ag+/TiO_2, J. Environ. Sci. 26 (2014) 662–672.
[40] X. Wang, W. Hou, D. Li, K. Yao, The antibacterial and hydrophilic properties of silver-doped TiO_2 thin films using sol?gel method, Appl. Surf. Sci. 258 (2012) 8241–8246.
[41] X. Pan, I. Medina-Ramirez, R. Mernaugh, J. Liu, Nanocharacterization and bactericidal performance of silver modified titania photocatalyst, Colloids Surf. B Biointerfaces 77 (2010) 82–89.
[42] A. Sirelkhatim, S. Mahmud, A. Seeni, N.H.M. Kaus, L.C. Ann, S.K.M. Bakhori, H. Hasan, D. Mohamad, Review on zinc oxide nanoparticles: antibacterial activity and toxicity mechanism, Nano-Micro Letters 7 (2015) 219–242.
[43] Lakshmi Prasanna, V.R. Vijayaraghavan, Insight into the mechanism of antibacterial activity of ZnO: surface defects mediated reactive oxygen species even in the dark, Langmuir: ACS J. Surf. Colloids 31 (2015) 9155–9162.
[44] J. Song, H. Kim, Y. Jang, J. Jang, Enhanced antibacterial activity of silver/polyrhodanine-composite-decorated silica nanoparticles, ACS Appl. Mater. Interfaces 5 (2013) 11563–11568.
[45] J.P. Ruparelia, A.K. Chatterjee, S.P. Duttagupta, S. Mukherji, Strain specificity in antimicrobial activity of silver and copper nanoparticles, Acta Biomater. 4 (2008) 707–716.
[46] B. Jia, Y. Mei, L. Cheng, J. Zhou, L. Zhang, Preparation of copper nanoparticles coated cellulose films with antibacterial properties through one-step reduction, ACS Appl. Mater. Interfaces 4 (2012) 2897–2902.